

# Artificial precession and instability in solar system and planetary simulations: analytic and numerical results

DAVID M. HERNANDEZ <sup>1</sup>

<sup>1</sup>*Department of Physics, National Taiwan Normal University, Taipei 116, Taiwan*

## ABSTRACT

Wisdom–Holman (WH) methods are algorithms used as a basis for a wide range of codes used to solve problems in solar system and planetary dynamics. The problems range from the growth and migration of planets to the stability of the solar system. In many cases, these codes work with Democratic Heliocentric Coordinates (DHC) which offer some advantages. However, it has been noted these coordinates affect the dynamics of solar system bodies in simulations, in particular Mercury’s, and introduce artificial precession which affects solar system stability. In this work, we analytically derive the two-body artificial precession induced by DHC. We show the effect is small for solar system bodies, but the artificial effect on Jupiter is 242 times larger than on Mercury. In a two-body Mercury–Sun system with general relativity (GR), artificial precession is negligible compared to GR precession, even with extreme timesteps that amplify the numerical effects. In a full solar system model, numerical effects are amplified further.

*Keywords:* N-body simulations (1083) — Celestial mechanics (211) — Computational methods (1965) — Solar system evolution (2293) — Planetary system evolution (2292)

## 1. INTRODUCTION

In studies over many dynamical timescales, planetary, planetesimal, and solar system dynamics usually use specialized algorithms based on the Wisdom–Holman (WH) method (H. Kinoshita et al. 1991; J. Wisdom & M. Holman 1991). These codes are used for studies ranging from stability analyses, to the growth of planets and planetary accretion, to the migration of planets. The idea behind WH is simple: most planetary motion can be treated as a Keplerian two-body problem. Perturbations from additional forces and planets are treated as a small effect, added in after two-body solutions.

Democratic Heliocentric Coordinates (DHC) (M. J. Duncan et al. 1998) are used in many such codes, like WHFast512 (P. Javaheri et al. 2023), MERCURY and MERCURIUS (J. E. Chambers 1999; H. Rein et al. 2019), SYMBA (M. H. Lee et al. 1997; M. J. Duncan et al. 1998; H. F. Levison & M. J. Duncan 2000), GENGA (S. L. Grimm & J. G. Stadel 2014), HNBODY (K. P. Rauch & D. P. Hamilton 2002), and TRACE, (D. M. Hernandez & W. Dehnen 2023; T. Lu et al. 2024). Originally, WH was developed using Jacobi coordinates, which has advantages and disadvantages; for an overview see D. M.

Hernandez & W. Dehnen (2017); H. Rein & D. Tamayo (2019). A disadvantage of DHC is that WH in DHC does not solve two-body problems exactly, in contrast to WH in Jacobi coordinates.

R. E. Zeebe (2015) noted that the evolution of Mercury’s eccentricity in simulations of the solar system depended on the coordinate system. N. A. Kaib & S. N. Raymond (2025) found the solar system was significantly more stable when using DHC. H. Rein et al. (2026) have proposed an explanation for this stability in that WH in DHC introduces artificial precession to Mercury’s orbit, in the same prograde direction as general relativity (GR), which pushes the  $g_1$  secular frequency associated with Mercury ( $= 559''/\text{cent}$ ) further from  $g_5 = 426''/\text{cent}$ , associated with Jupiter.  $g_1$  evolves subdiffusively in time (D. S. Abbot et al. 2024), and solar system instabilities are associated with the case of  $g_1$  approaching  $g_5$ .

In this paper, we derive and test the artificial two-body precession due to WH in DHC. We find a small effect that is 242 times stronger for Jupiter than for Mercury. We also test two-body artificial precession in the presence of GR, finding a negligible effect, even for extreme timesteps. Finally, we can match the qualitative H. Rein et al. (2026) strong artificial precession results with a simplified two-planet system.

Section 2 presents mathematical preliminaries. In Section 3 we derive and test two-body artificial precession. Section 4 studies two-body problems in the presence of GR. We conclude in Section 5.

## 2. MATHEMATICAL PRELIMINARIES

A system of  $N$  point particles subject to Newtonian gravitational forces has Hamiltonian, written in inertial Cartesian coordinates,

$$H = T + V = \sum_{i=0}^{N-1} \frac{\mathbf{p}_i^2}{2m_i} - \sum_{i=0}^{N-1} \sum_{j=i+1}^{N-1} \frac{Gm_i m_j}{r_{ij}}, \quad (1)$$

where we've identified the kinetic and potential energies,  $T$  and  $V$ .  $G$  is Newton's gravitational constant,  $\mathbf{p}_i$  is the non-relativistic momentum of particle  $i$ ,  $m_i$  its mass, and  $\mathbf{r}_i$  its position.  $\mathbf{r}_{ij} = \mathbf{r}_i - \mathbf{r}_j$ . Angular momentum  $\mathbf{L} = \sum_i \mathbf{r}_i \times \mathbf{p}_i$  is conserved by Hamiltonian (1).

Given a phase space state of a system of particles described by (1), our goal is to calculate the state at a time  $t$ . Assume the state at  $t = 0$  is  $\mathbf{z}(0) = (\mathbf{r}(0), \mathbf{p}(0))$ . Hamilton's equations are difficult to solve:

$$\begin{aligned} \dot{\mathbf{p}}_i &= -G \sum_{j \neq i} \frac{m_i m_j}{r_{ij}^3} \mathbf{r}_{ij}, \\ \dot{\mathbf{r}}_i &= \frac{\mathbf{p}_i}{m_i}. \end{aligned} \quad (2)$$

To arrive at the same result, we can use a different mathematical formulation. Given a function  $F(\mathbf{z})$ , define an operator  $\hat{F}\mathbf{z} = \{\mathbf{z}, F\}$ , where  $\{\}$  are Poisson brackets:

$$\{K, F\} = \sum_i \left( \frac{\partial K}{\partial \mathbf{r}_i} \cdot \frac{\partial F}{\partial \mathbf{p}_i} - \frac{\partial K}{\partial \mathbf{p}_i} \cdot \frac{\partial F}{\partial \mathbf{r}_i} \right), \quad (3)$$

with  $K$  a second function of  $\mathbf{z}$ . Any canonical basis, not just Cartesian coordinates, can be used to compute derivatives in Eq. (3). Hamilton's equations are then,

$$\dot{\mathbf{z}} = \{\mathbf{z}, H\}. \quad (4)$$

It follows that  $F = \{F, H\}$ . The solution to Hamilton's equations is given by the infinite series,

$$\mathbf{z}(t) = \exp\left(t\hat{H}\right) \mathbf{z}(0) = \sum_{i=0}^{\infty} \frac{t^i}{i!} \hat{H}^i \mathbf{z}(0). \quad (5)$$

Obviously, solution (5) is not very useful or practical. A simpler, but approximate, solution path is often taken in dynamical systems work. We separate Hamiltonian (1) into two or more pieces that are easier to solve and often integrable. This approach yields what is known as a symplectic integrator. If the masses in (1) are not too different in scale, some approaches are given by G. Gonçalves Ferrari et al. (2014); D. M. Hernandez & E. Bertschinger (2015); W. Dehnen & D. M. Hernandez

(2017). In this paper, however, we specialize to the case when  $m_0 \gg m_{i>0}$ . We call  $m_0$  the ‘‘star’’ and  $m_{i>0}$  ‘‘planets.’’ As an example of such a splitting, let  $H = A_C + B_C$ , with,

$$\begin{aligned} A_C &= \sum_{i \neq 0} \frac{\mathbf{p}_i^2}{2m_i} - \frac{Gm_0 m_i}{r_{i0}} \quad \text{and} \\ B_C &= \frac{\mathbf{p}_0^2}{2m_0} - \sum_{0 < i < j} \frac{Gm_i m_j}{r_{ij}}. \end{aligned} \quad (6)$$

$A_C$  is a sum of  $n$  independent Kepler two-body problems, with  $n = N - 1$  the number of planets. Extensive tools are available to solve  $A_C$ .  $B_C$  is a trivial integrable Hamiltonian. Solving  $B_C$  maps state  $\mathbf{z}$  at  $t = 0$  to  $\mathbf{z}'$  at  $t$ :

$$\begin{aligned} \mathbf{p}'_{i>0} &= \mathbf{p}_{i>0} - t \sum_{j \neq i, j > 0} \frac{Gm_i m_j}{r_{ij}^3} \mathbf{r}_{ij}, \\ \mathbf{r}'_0 &= \mathbf{r}_0 + t \frac{\mathbf{p}_0}{m_0}. \end{aligned} \quad (7)$$

In a barycentric frame,  $B_C/A_C = \mathcal{O}(\epsilon)$ , with

$$\epsilon = \max(m_i/m_0), \quad (8)$$

a small parameter. To see this, use the scaling arguments,  $v_i^2 \propto m_0/r_{i0}$  and  $p_0^2 \propto m_i^2 v_i^2$ , with  $\mathbf{v}_i = \dot{\mathbf{r}}_i$ .

Having effectuated our Hamiltonian splitting (6), rather than using Eq. (5), we write the approximate solution,

$$\mathbf{z}(t) = \exp(t\hat{A}_C) \exp(t\hat{B}_C) \mathbf{z}(0) = \exp(t\hat{H}_{\text{Eul}}) \mathbf{z}(0), \quad (9)$$

which is only a good approximation for  $t$  small.  $\hat{H}_{\text{Eul}}$  is a surrogate Hamiltonian, close to  $H$  for small  $t$ :

$$\hat{H}_{\text{Eul}} = H + tH_1 + t^2H_2 + \dots, \quad (10)$$

where the  $H_i$  can be computed via the Baker–Campbell–Hausdorff (BCH) formula (J. Campbell 1896, 1897; H. F. Baker 1902, 1905; F. Hausdorff 1906; E. Dynkin 1947; E. Hairer et al. 2006).

We can do better still than Eq. (9) in our approximation to  $\mathbf{z}(t)$ . We first find a better canonical coordinate system that reduces the number of degrees of freedom. A suitable choice is DHC, written  $(\mathbf{Q}, \mathbf{P})$ .  $\mathbf{Q}_0$  and  $\mathbf{P}_0$  are the center of mass and total momentum, respectively, while  $\mathbf{Q}_{i>0}$  and  $\mathbf{P}_{i>0}$  are heliocentric positions and barycentric momenta, respectively. We obtain

these coordinates via linear transformations,

$$\mathbf{Q}_0 = \sum_j \frac{m_j}{M} \mathbf{r}_j, \quad (11a)$$

$$\mathbf{Q}_{i \neq 0} = \mathbf{r}_i - \mathbf{r}_0, \quad (11b)$$

$$\mathbf{P}_0 = \sum_j \mathbf{p}_j, \quad (11c)$$

$$\mathbf{P}_{i \neq 0} = \mathbf{p}_i - \frac{m_i}{M} \mathbf{P}_0 = \mathbf{p}_i - \frac{m_i}{M} \sum_j \mathbf{p}_j, \quad (11d)$$

with  $M = \sum_i m_i$ . In DHC, working in a barycentric frame, we can write,

$$H = \underbrace{\sum_{i \neq 0} \frac{\mathbf{P}_i^2}{2m_i}}_{T_1} + \underbrace{\frac{1}{2m_0} \left( \sum_{i \neq 0} \mathbf{P}_i \right)^2}_{T_0} - \underbrace{\sum_{i \neq 0} \frac{Gm_i m_0}{|\mathbf{Q}_i|}}_{V_\odot} - \underbrace{\sum_{0 < i < j} \frac{Gm_i m_j}{|\mathbf{Q}_i - \mathbf{Q}_j|}}_{V_{\text{pl}}}, \quad (12)$$

where we identified functions  $T_1$ ,  $T_0$ ,  $V_\odot$ , and  $V_{\text{pl}}$ , equal to the planetary kinetic energies, solar kinetic energy, potential energy from Sun-planet interactions, and potential energy from planet-planet interactions, respectively. It is easy to show,

$$\mathbf{L} = \sum_i \mathbf{r}_i \times \mathbf{p}_i = \sum_i \mathbf{Q}_i \times \mathbf{P}_i, \quad (13)$$

and,

$$\{\mathbf{L}, T_1\} = \{\mathbf{L}, T_0\} = \{\mathbf{L}, V_\odot\} = \{\mathbf{L}, V_{\text{pl}}\} = 0 : \quad (14)$$

all the functions conserve  $\mathbf{L}$ .

The next improvement comes from increasing the order of the error in Eq. (10) from  $t^1$  to  $t^2$ . Now, using a small timestep  $h$ , we can write as solution,

$$\begin{aligned} \mathbf{z}(h) &= \exp\left(\frac{h}{2} \hat{A}_D\right) \exp\left(h \hat{B}_D\right) \exp\left(\frac{h}{2} \hat{A}_D\right) \mathbf{z}(0) \\ &= \exp\left(h \hat{H}_{\text{ABA}}\right) \mathbf{z}(0), \end{aligned} \quad (15)$$

with,

$$A_D = T_1 + V_\odot \quad \text{and} \quad B_D = T_0 + V_{\text{pl}}. \quad (16)$$

If  $t = mh$ ,  $\mathbf{z}(t)$  is then found by iterating Eq. (15) for  $m$  steps. We can show again that  $B_D/A_D = \mathcal{O}(\epsilon)$ . Eq. (15) is the ‘‘ABA’’ second order method; just as valid, we can construct a ‘‘BAB’’ method by swapping  $A_D$  and

$B_D$ .  $\tilde{H}_{\text{BAB}}$  and  $\tilde{H}_{\text{ABA}}$  are closer to  $H$  than  $\tilde{H}_{\text{Eul}}$ :

$$\tilde{H}_{\text{BAB}} = H + \frac{h^2}{12} \{\{B_D, A_D\}, A_D\} \quad (17)$$

$$- \frac{h^2}{24} \{\{A_D, B_D\}, B_D\} + \mathcal{O}(h^4),$$

$$\tilde{H}_{\text{ABA}} = H - \frac{h^2}{24} \{\{B_D, A_D\}, A_D\} \quad (18)$$

$$+ \frac{h^2}{12} \{\{A_D, B_D\}, B_D\} + \mathcal{O}(h^4).$$

If we let  $A_D \propto \epsilon^0$ , then  $B_D \propto \epsilon^1$  and  $\mathbf{P}_{i \neq 0} \propto \epsilon^0$ , so that a Poisson bracket does not change the order of  $\epsilon$ . This leads us to find the leading order error for Eqs. (17) and (18) is  $\mathcal{O}(\epsilon h^2)$ . We can write the error terms in more detail:

$$\{\{A_D, B_D\}, B_D\} = \{\{V_\odot, T_0\}, T_0\} + \{\{T_1, V_{\text{pl}}\}, V_{\text{pl}}\}, \quad \text{and} \quad (19a)$$

$$\begin{aligned} \{\{B_D, A_D\}, A_D\} &= \{\{T_0, V_\odot\}, V_\odot\} + \{\{V_{\text{pl}}, T_1\}, T_1\} \\ &\quad - \{\{T_1, V_{\text{pl}}\}, V_\odot\} - \{\{V_\odot, T_0\}, T_1\}. \end{aligned} \quad (19b)$$

The explicit forms for Eqs. (19) in terms of  $(\mathbf{Q}, \mathbf{P})$  are presented in (D. M. Hernandez & W. Dehnen 2017, Eqs. 41). Both methods ABA and BAB form the basis of the list of codes in Section 1.

### 3. TWO-BODY PRECESSION

Now, consider the case of two bodies, when  $V_{\text{pl}} = 0$ . Eqs. (19) simplify:

$$\{\{A_D, B_D\}, B_D\} = \{\{V_\odot, T_0\}, T_0\}, \quad \text{and} \quad (20a)$$

$$\{\{B_D, A_D\}, A_D\} = \{\{T_0, V_\odot\}, V_\odot\} - \{\{V_\odot, T_0\}, T_1\}. \quad (20b)$$

The fact that  $\tilde{H}_{\text{BAB}}$  and  $\tilde{H}_{\text{ABA}}$  are not exactly equal to  $H$  implies the two-body problem is not solved exactly. However,  $\tilde{H}_{\text{BAB}}$  and  $\tilde{H}_{\text{ABA}}$  are conserved for  $h$  small, and  $\mathbf{L}$  is exactly conserved per Eq. (14): the end result is a two-body precessing orbit. We can say that the motion is integrable, but not superintegrable (F. Fassò 2005).

We can calculate, say, Eq. (17) explicitly, using eqs. 41 from D. M. Hernandez & W. Dehnen (2017). There are only 3 degrees of freedom,  $(\mathbf{Q}_1, \mathbf{P}_1)$ , which we denote simply as  $(\mathbf{Q}, \mathbf{P})$ :

$$\begin{aligned} \tilde{H}_{\text{BAB}} &= \frac{P^2}{2\mu} - \frac{Gm_0 m_1}{Q} - \frac{Gh^2 \epsilon}{24} \left( \frac{P^2}{Q^3} - \frac{3(\mathbf{P} \cdot \mathbf{Q})^2}{Q^5} \right) \\ &\quad + \frac{Gh^2}{12} \left( \frac{Gm_0 m_1^2}{Q^4} + \frac{P^2}{Q^3} - \frac{3(\mathbf{P} \cdot \mathbf{Q})^2}{Q^3} \right) + \mathcal{O}(h^4), \end{aligned} \quad (21)$$

where  $\mu = m_0 m_1 / (m_0 + m_1)$  is called the reduced mass, and

$$\epsilon = m_1 / m_0, \quad (22)$$

from Eq. (8).

In a barycentric frame, Eq. (1) is,

$$H = \frac{p_r^2}{2\mu} - \frac{Gm_0 m_1}{r_{01}} = \frac{P^2}{2\mu} - \frac{Gm_0 m_1}{Q}, \quad (23)$$

where  $\mathbf{p}_r = \mu(\mathbf{v}_1 - \mathbf{v}_0) = \mu(\mathbf{P}/m_1 + \mathbf{P}/m_0) = \mathbf{P}$ . The Runge–Lenz (RL) vector is,

$$\mathbf{R} = \mathbf{P} \times \mathbf{L} - c_0 \frac{\mathbf{Q}}{Q}, \quad (24)$$

with  $c_0 = Gm_0^2 m_1^2 / M$ .  $\mathbf{R}$  points from the barycenter to periapse and

$$\{\mathbf{R}, H\} = 0. \quad (25)$$

An instantaneous and average precession rate is constructed:

$$\dot{\omega} = \frac{(\mathbf{R} \times \dot{\mathbf{R}})_z}{R^2} \quad \text{and} \quad \langle \dot{\omega} \rangle = \left\langle \frac{(\mathbf{R} \times \dot{\mathbf{R}})_z}{R^2} \right\rangle, \quad (26)$$

where a  $z$  subscript indicates we take the  $z$ -component, and  $\hat{z}$  is defined as  $\hat{\mathbf{L}}$ . Time averages are carried out by integrating over the orbit defined by  $H$ , which is the BAB orbit plus a correction of  $\mathcal{O}(h^2)$ , per Eq. (21). Thus, our numerical BAB orbit yields,

$$R^2 = c_0^2 e^2 + \mathcal{O}(h^2) \quad \text{and} \quad \mathbf{R} = \mathbf{R}_0 + \mathcal{O}(h^2), \quad (27)$$

with  $e$  and  $\mathbf{R}_0$  the eccentricity and invariant RL vector described by  $H$ . The difference between the BAB and  $H$  semi-major axes,  $a_{\text{BAB}} - a$ , remains small over exponentially long times (E. Hairer et al. 2006, Sec. IX.8, Thm. 8.1); this is a fundamental property of symplectic methods (P. J. Channell & C. Scovel 1990; J. Sanz-Serna & M. Calvo 1994; B. Leimkuhler & S. Reich 2004; S. Blanes & F. Casas 2017; S. Tremaine 2023). Moreover,  $\mathbf{L}$  is exactly conserved by  $H$  and  $\tilde{H}_{\text{BAB}}$ . It can be written,

$$L = \mu \sqrt{GMa(1 - e^2)}, \quad (28)$$

which implies  $e - e_{\text{BAB}}$  also cannot drift secularly in time. This can be numerically verified.

Next,

$$\dot{\mathbf{R}} = \{\mathbf{R}, \tilde{H}_{\text{BAB}}\} = \{\mathbf{R}, H_{\text{err}}\}, \quad (29)$$

where  $H_{\text{err}} = \tilde{H}_{\text{BAB}} - H$  is the error Hamiltonian. With manipulation of Eqs. (17) and (19), we can write,

$$H_{\text{err}} = \underbrace{\frac{h^2}{24} [\{V_\odot, T_0\}, H]}_{H_A} + \underbrace{\frac{h^2}{24} [\{V_\odot, T_0\}, T_0]}_{H_B} + \mathcal{O}(h^4),$$

(30)

where we have identified  $H_A$  and  $H_B$ . The Jacobi identity for Poisson brackets, for  $F(\mathbf{z})$ ,  $J(\mathbf{z})$ , and  $K(\mathbf{z})$ , is,

$$\{F, \{J, K\}\} + \{J, \{K, F\}\} + \{K, \{F, J\}\} = 0. \quad (31)$$

Using it, and Eq. (25), we find,

$$\begin{aligned} \{\mathbf{R}, H_A\} &= \{\mathbf{R}, \{S, H\}\} = -\{S, \{H, \mathbf{R}\}\} - \{H, \{\mathbf{R}, S\}\} \\ &= \frac{d}{dt} (\{\mathbf{R}, S\}), \end{aligned} \quad (32)$$

where  $S = (h^2/24)\{V_\odot, T_0\}$  and the time derivative is along the orbit described by  $H$ .

To leading order in  $h$ ,  $\mathbf{R} \times \dot{\mathbf{R}} = \mathbf{R}_0 \times \dot{\mathbf{R}}$  and the average precession over an orbit contributed by Eq. (32) must be 0 as the orbit is periodic. Thus, only  $H_B$  contributes to precession:

$$\begin{aligned} \dot{\mathbf{R}} &= \{\mathbf{R}, H_B\} = \frac{Gh^2\epsilon}{24} \left\{ \mathbf{P} \times \mathbf{L} - c_0 \frac{\mathbf{Q}}{Q}, \frac{P^2}{Q^3} - \frac{3(\mathbf{P} \cdot \mathbf{Q})^2}{Q^5} \right\} \\ &\quad + \mathcal{O}(h^4). \end{aligned} \quad (33)$$

Because of (14),  $\mathbf{L}$  can be taken outside all Poisson brackets. The result of Eq. (33) is straightforward:

$$\begin{aligned} \dot{\mathbf{R}} &= \frac{Gh^2\epsilon}{24} \left[ (\mathbf{Q} \times \mathbf{L}) \left( \frac{3P^2}{Q^5} - \frac{15(\mathbf{P} \cdot \mathbf{Q})^2}{Q^7} + \frac{4c_0}{Q^6} \right) \right. \\ &\quad \left. + (\mathbf{P} \times \mathbf{L}) \frac{6(\mathbf{P} \cdot \mathbf{Q})}{Q^5} - \frac{2c_0 \mathbf{P}}{Q^4} + \frac{2c_0(\mathbf{P} \cdot \mathbf{Q})\mathbf{Q}}{Q^6} \right] + \mathcal{O}(h^4). \end{aligned} \quad (34)$$

We then compute the cross product, and take the  $z$  component:

$$\begin{aligned} (\mathbf{R} \times \dot{\mathbf{R}})_z &= \frac{Gh^2\epsilon L}{24} \\ &\quad \times \left[ (-L^2 + c_0 Q) \left( \frac{3P^2}{Q^5} - \frac{15(\mathbf{P} \cdot \mathbf{Q})^2}{Q^7} + \frac{4c_0}{Q^6} \right) \right. \\ &\quad \left. + \frac{8c_0(\mathbf{P} \cdot \mathbf{Q})^2}{Q^6} - \frac{2c_0}{Q^4} \left( P^2 - \frac{c_0}{Q} \right) \right] + \mathcal{O}(h^4), \end{aligned} \quad (35)$$

Using Eqs. (26), (27), and (28),

$$\begin{aligned} \dot{\omega} &= \frac{Gh^2\epsilon\sqrt{c_0 a(1 - e^2)}}{24e^2} \\ &\quad \times \left[ (-a(1 - e^2) + Q) \left( \frac{3v^2}{GMQ^5} - \frac{15(\mathbf{v} \cdot \mathbf{Q})^2}{GMQ^7} + \frac{4}{Q^6} \right) \right. \\ &\quad \left. + \frac{8(\mathbf{v} \cdot \mathbf{Q})^2}{GMQ^6} - \frac{2}{Q^4} \left( \frac{v^2}{GM} - \frac{1}{Q} \right) \right] + \mathcal{O}(h^4), \end{aligned} \quad (36)$$

where  $\mathbf{v} = \mathbf{P}/\mu$  is the relative velocity.

Next, we must compute the average over a period for Eq. (36). Writing the expressions for  $\mathbf{v}(t)$  and  $\mathbf{Q}(t)$  for a two-body orbit, and converting to an average over true anomaly, the following time averages are computed:

$$\left\langle \frac{v^2}{Q^5} \right\rangle = \frac{GM}{a^6} \frac{4 + 22e^2 + 9e^4}{4(1 - e^2)^{9/2}}, \quad (37a)$$

$$\left\langle \frac{v^2}{Q^4} \right\rangle = \frac{GM}{a^5} \frac{2 + 7e^2 + e^4}{2(1 - e^2)^{7/2}}, \quad (37b)$$

$$\left\langle \frac{(\mathbf{v} \cdot \mathbf{Q})^2}{Q^7} \right\rangle = \frac{GM e^2}{a^6} \frac{4 + 3e^2}{8(1 - e^2)^{9/2}}, \quad (37c)$$

$$\left\langle \frac{(\mathbf{v} \cdot \mathbf{Q})^2}{Q^6} \right\rangle = \frac{GM e^2}{a^5} \frac{4 + e^2}{8(1 - e^2)^{7/2}}, \quad (37d)$$

$$\left\langle \frac{1}{Q^6} \right\rangle = \frac{1}{a^6} \frac{8 + 24e^2 + 3e^4}{8(1 - e^2)^{9/2}}, \quad (37e)$$

$$\left\langle \frac{1}{Q^5} \right\rangle = \frac{1}{a^5} \frac{2 + 3e^2}{2(1 - e^2)^{7/2}}. \quad (37f)$$

Taking an average of Eq. (36) is then,

$$\langle \dot{\omega} \rangle = -\frac{h^2}{4} \epsilon \left( \frac{m_0 m_1}{M^2} \right) \left( \frac{GM}{a^3} \right)^{3/2} \frac{1 + \frac{\epsilon^2}{4}}{(1 - e^2)^3} + \mathcal{O}(h^4), \quad (38)$$

or, preferring  $m_0$  rather than  $M$ ,

$$\langle \dot{\omega} \rangle = -\frac{h^2}{4} \epsilon^2 \omega_0^3 \frac{1 + \frac{\epsilon^2}{4}}{(1 - e^2)^3} + \mathcal{O}(\epsilon^3 h^2 + h^4), \quad (39)$$

with  $\omega_0 = (Gm_0/a^3)^{1/2}$  and  $\epsilon$  from Eq. (22). Note the negative sign, indicating the precession is always retrograde. The artificial precession goes to 0 as the timestep is decreased to 0. It also grows with  $\omega_0$ . As  $e \rightarrow 1$ ,  $\langle \dot{\omega} \rangle$  increases sharply; however, our averaging result may break down as the map may not sample pericenter well.

### 3.1. What about ABA?

We now calculate the precession frequency for the dual map ABA. Letting  $\Delta H = \tilde{H}_{ABA} - \tilde{H}_{BAB}$ , Eqs. (17) and (18) say,

$$\Delta H = \frac{h^2}{8} \{ \{ A_D, B_D \}, H \} + \mathcal{O}(h^4). \quad (40)$$

Defining,  $\Delta \dot{\mathbf{R}} = \dot{\mathbf{R}}_{ABA} - \dot{\mathbf{R}}_{BAB}$ , we get, using Eqs. (31) and (25).

$$\begin{aligned} \Delta \dot{\mathbf{R}} &= \frac{h^2}{8} \{ \mathbf{R}, \{ \{ A_D, B_D \}, H \} \} + \mathcal{O}(h^4) \\ &= \frac{h^2}{8} \{ H, \{ \{ A_D, B_D \}, \mathbf{R} \} \} + \mathcal{O}(h^4) \\ &= -\frac{h^2}{8} \frac{d}{dt} \{ \{ A_D, B_D \}, \mathbf{R} \} + \mathcal{O}(h^4). \end{aligned} \quad (41)$$

Using the same logic as that under Eq. (32), we see,

$$\left\langle \dot{\mathbf{R}}_{ABA} \right\rangle = \left\langle \dot{\mathbf{R}}_{BAB} \right\rangle + \mathcal{O}(h^4), \quad (42)$$

so that expression (39) is valid for ABA as well.

### 3.2. Numerical verification

To verify Eq. (39), we set up a two-body system, initialized at apocenter, with  $\mathbf{r}_{10} = a(1 + e)\hat{x}$  and  $\dot{\mathbf{r}}_{10} = \sqrt{GM(1 - e)/(a(1 + e))}\hat{y}$  so that  $\dot{\mathbf{R}}(0) = -\hat{x}$ . We use BAB to solve for the motion in time. In units of solar mass, au, and yr, we set  $m_0 = 1$ ,  $m_1 = 0.001$ ,  $a = 1$ .  $e$  is chosen as 25 linearly spaced values between 0.1 and 0.8.  $h = P/100$ , where  $P = 1.00$  is the period. We run for  $t_{\max} = 10^4 P$ . The angle  $\theta$  of  $\mathbf{R}$  with  $\mathbf{R}(0)$  is calculated at every step, with the orientation of  $\theta$  determined by  $\hat{\mathbf{L}}$ . Numerically,  $\theta$  is found to decrease linearly in time over  $t_{\max}$ ; however, on short timescales there are departures from linearity due to numerical artifacts of the timestep interacting with timescales in the system; such numerical artifacts are well-known and average out over longer timescales. Thus, we define

$$\langle \dot{\omega}_{\text{num}} \rangle = \Delta\theta/t_{\max}. \quad (43)$$

As predicted by (39), we find the precession to be retrograde, regardless of the orientation of  $\hat{\mathbf{L}}$ . We check the scaling of (39) with  $e$ , written  $g = (1 + e^2/4)/(1 - e^2)^3$ . Let  $x = 1 - e^2$ . Then, we find the slope,

$$s = \frac{d \log g}{d \log x} = -3 - \frac{x/4}{1 + 1/4(1 - x)}, \quad (44)$$

so that  $s \in [-3.25, -3]$  as  $e$  increases from 0 to 1. Figure 1 plots  $\log x$  versus  $\log \langle \dot{\omega}_{\text{num}} \rangle$ . For the data excluding the smallest two  $x$  values,  $e \leq 0.74$ ,  $s = -3.21$  fits the data well, as seen in Fig. 1. A least squares fit for these data without the two points yields  $s = -3.21$ . As  $e \rightarrow 0$  (ignoring higher order terms),  $\langle \dot{\omega} \rangle = -h^2 \epsilon^2 \omega_0^3 / 4 = -0.13''/\text{cent}$ .

For  $e > 0.74$  (two smallest  $x$  points of Fig. 1), there is a clear change of slope, which we verified by testing smaller  $x$  than those shown, although the scaling with  $h^2$  remains. However, agreement with (39) is reestablished if we reduce  $h$  further. Changing the initial phase to pericenter also improves agreement with theory up to  $e = 0.80$ . At high  $e$ , it's clear the derivation leading up to Eq. (39) no longer holds; in particular our uniform averaging over the time likely doesn't hold due to fast pericenter passages.

Fig. 2 plots the relative error between the predicted precession ( $\langle \dot{\omega} \rangle_{\text{an}}$ ) and  $\langle \dot{\omega} \rangle_{\text{num}}$  as a function of  $e$ . This plot tests the accuracy of the coefficients besides  $g$  in Eq. (39). The agreement is again good for  $e \leq 0.74$ , with minimum error  $\approx 10^{-3} = \epsilon$ . All scalings with  $m_0$ ,

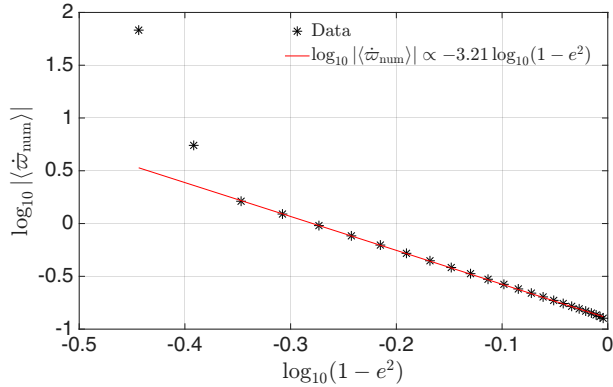


**Figure 1.** Numerical verification of the dependence on eccentricity of the two-body precession rate, Eq. (39). In units of solar mass, au, and yr, we let  $m_0 = 1$ ,  $m_1 = 0.001$ ,  $a = 1$ ,  $h = P/100$ ,  $P = 1.00$ , and  $t_{\max} = 10^4 P$ , where  $t_{\max}$  is the runtime. The expected slope of  $\log_{10}(1 - e^2)$  versus  $\log_{10} \langle \dot{\varpi}_{\text{num}} \rangle$  is  $s \in [-3.25, -3]$  as  $e$  is increased to 1. At large  $e$ ,  $e > 0.74$ , our precession derivation breaks down. A least squares  $s = -3.21$  for  $e \leq 0.74$  is plotted, and is consistent with theory.

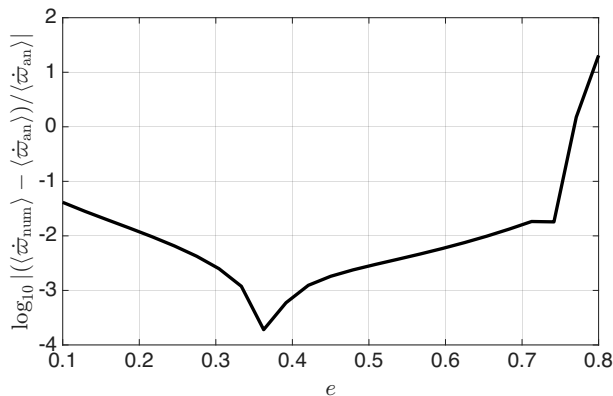


**Figure 2.** The relative error between the predicted ( $\langle \dot{\varpi} \rangle_{\text{an}}$ ) and numerical ( $\langle \dot{\varpi} \rangle_{\text{num}}$ ) precession rate as a function of  $e$ . The system and parameters are the same as those for Fig. 1. While Fig. 1 tests the scaling with  $e$ , here we test the full Eq. (39). The agreement is good for  $e \leq 0.74$ , and agreement at higher  $e$  is reestablished with smaller timesteps.

$a$ , and  $m_1$  have been checked and we verified BAB and ABA have no significant differences in their numerical precessions.

We can test Eq. (39) in the context of the solar system with its current orbital parameters. The precession associated with Mercury is  $g_1 = 559''/\text{cent}$ , while  $g_5$ , associated with Jupiter, is  $g_5 = 426''/\text{cent}$ . Choosing  $h = 4$  days, Eq. (39) predicts average precession rates, which we can use as proxies for an artificial secular frequency,  $\tilde{g}_i$ :  $\tilde{g}_1 = -3.5 \times 10^{-7}''/\text{cent}$  and  $\tilde{g}_5 = -8.4 \times 10^{-5}''/\text{cent}$ , both minuscule amounts.

However, it's noteworthy the impact on Jupiter is 242 times larger than on Mercury, due to the  $e^2$  effect.

#### 4. GENERAL RELATIVISTIC CORRECTIONS AND PLANET-PLANET INTERACTIONS

General relativity is often incorporated into solar system simulations as a position-dependent potential:

$$V_{\text{GR}} = -\frac{3G^2 m_0^2 m_1}{c^2 Q^2}, \quad (45)$$

(A. Nobili & I. W. Roxburgh 1986; P. Saha & S. Tremaine 1992; D. Tamayo et al. 2020), where  $c$  is the speed of light. H. Rein et al. (2026) and N. A. Kaib & S. N. Raymond (2025) used this form. The total Hamiltonian is now,

$$H = T_1 + T_0 + V_{\odot} + V_{\text{pl}} + V_{\text{GR}}. \quad (46)$$

We can calculate the physical, not artificial, precession due to  $V_{\text{GR}}$  by using Eq. (26).  $H$  and  $L$ , or  $e$  and  $a$ , are conserved so  $R$  is constant. We use Eq. (26) and

$$\begin{aligned} \left\langle \frac{1}{Q^3} \right\rangle &= \frac{1}{a^3(1 - e^2)^{3/2}}, \\ \left\langle \frac{1}{Q^4} \right\rangle &= \frac{2 + e^2}{2a^4(1 - e^2)^{5/2}}. \end{aligned} \quad (47)$$

Then, we have,

$$\langle \dot{\varpi} \rangle = \frac{3G^{3/2} m_0 M^{1/2}}{c^2 a^{5/2} (1 - e^2)}. \quad (48)$$

The direction is prograde, opposite the artificial contribution from earlier. To find the size of  $V_{\text{GR}}$ , use the same scaling arguments as those below map (7) to find, for Mercury,

$$V_{\text{GR}}/T_0 = \mathcal{O}((v_1^2/c^2)/(m_1/m_0)) = 10^{-1}, \quad (49)$$

Eq. (49) implies we can safely place  $V_{\text{GR}}$  in  $B_{\text{D}}$  for solar system simulations.

We now set up a two-body system consisting of Mercury and Sun:  $m_0 = 1$ ,  $m_1 = 1.66 \times 10^{-7}$ , and  $a = 0.387098$ , but  $e$  is set to 0.6 to match the second subplot of fig. 1 from H. Rein et al. (2026).  $P = 0.24085$  and  $t_{\max} = 10^5 P$ . We solve Hamiltonian (46) using BAB, comparing the numerical precession with Eq. (48).  $h$  is varied from  $h = 0.5$  to 60 days, again to match H. Rein et al. (2026). Timesteps beyond  $\approx 1$  day are not advised as they do not resolve pericenter in DHC (K. P. Rauch & M. Holman 1999; J. Wisdom 2015; D. M. Hernandez et al. 2022), although H. Rein et al. (2025) find that larger stepsizes can still successfully estimate some dynamics.

The result is shown in Fig. 3. We find excellent agreement between Eq. (48) and the numerical precession.

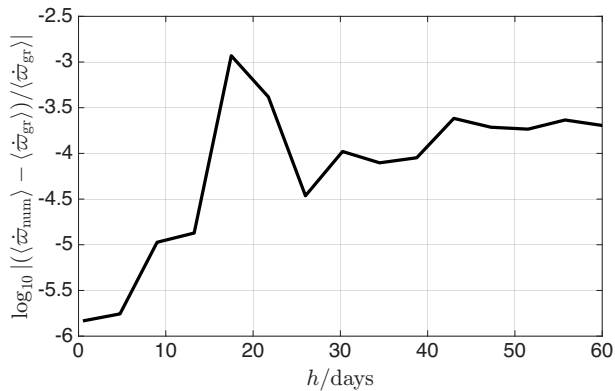


**Figure 3.** Error in numerical precession as compared to Eq. (48). A two-body problem consisting of Mercury and Sun, with  $e = 0.6$ , and a GR potential, is run. Even at large timesteps, artificial precession makes no significant impact.

This contrasts with the result from [H. Rein et al. \(2026\)](#), who find the precessions agree only up to  $h \approx 6$  days. The main difference between our simulations and theirs is their inclusion of  $V_{\text{pl}}$ , with all planets, so it is reasonable to conclude error terms, e.g., Eq. (19), that include  $V_{\text{pl}}$  are responsible for their artificial precession.  $V_{\text{pl}}$ , of course, is dependent on the exact planetary configuration under study.  $V_{\text{pl}}$  is responsible for most of  $g_1$ , so it is not unreasonable it would also be responsible for most artificial precession as well.

In fact, we’re able to qualitatively reproduce fig. 1, subplot 2, from [H. Rein et al. \(2026\)](#), with a simple experiment consisting of the Sun and two planets, with no GR. All motion is in a plane, and initially the planets’ arguments of pericenter are aligned and their phases are at aphelion. Their masses and semi-major axes are those of Mercury and Jupiter, respectively, but only Jupiter’s eccentricity matches its current value. Mercury’s eccentricity is set to 0.6. As in Fig. 3, we run for  $10^5 P$ , with  $P$  Mercury’s period. 15 timesteps are chosen, varying logarithmically between  $0.005P$  and  $0.8P$ , and a simulation is run with each. As we know for small  $h$  the artificial precession decreases with  $h^2$ , we choose  $h = 0.005P$  as the “analytic” simulation.

In Fig. 4 we plot the difference in average precession between the rest of simulations and the analytic run,  $\Delta$ , to obtain the artificial contribution. As in [H. Rein et al. \(2026\)](#), the artificial precession is prograde.  $\Delta \geq 95''/\text{cent}$  for  $h \geq 3.9$  days (except for  $h = 70$  days), surpassing the GR contribution to Mercury’s average precession, Eq. (48) ( $= 67''/\text{cent}$ ). The slope of  $\Delta$  for the 5 data points with  $h \leq 2.7$  days is 2.3, consistent within uncertainties with the expected  $h^2$  scaling.

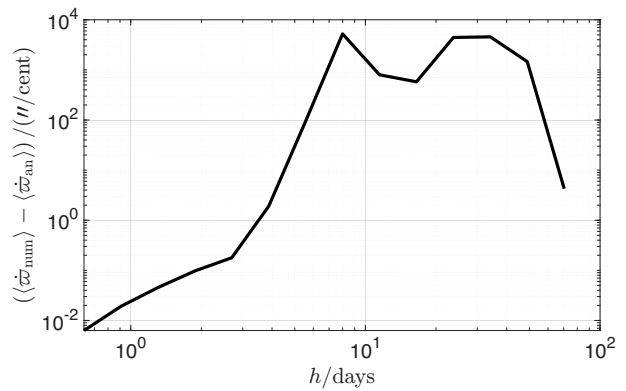


**Figure 4.** The artificial precession measured in a simplified two-planet Mercury–Jupiter system, as a function of timestep. Mercury’s eccentricity has been increased to  $e = 0.6$ , and there is no GR. Strong prograde artificial precession for  $h \geq 3.9$  days, surpassing the GR contribution (except at the last point), is found.

## 5. CONCLUSIONS

The Wisdom–Holman map in Democratic Heliocentric Coordinates, used extensively in studies of planetary dynamics, induces artificial precession for even a simple two-body problem. We derived the analytic form of this precession. Interestingly, the effects on Jupiter are far larger than on Mercury by a factor of 242 for present day orbital parameters. When running simulations that include general relativity (GR), the artificial precession is negligible compared to GR precession even when using extreme stepsizes.

Recently, [H. Rein et al. \(2026\)](#) found strong artificial precession for Mercury, matching the size of its GR precession, in their solar system studies. We have reproduced the important features of their result with a simplified Mercury–Jupiter system, strongly suggesting  $V_{\text{pl}}$  is responsible for our and their artificial precessions. Analytic study of artificial precession from  $V_{\text{pl}}$  depends on the specific planetary configuration. Our work sheds light on the origin of this artificial precession and suggests it may be an important effect on other bodies beyond Mercury.

## 6. ACKNOWLEDGEMENTS

D.M.H. acknowledges support from the National Science and Technology Council (NSTC) in Taiwan through grant 114-2112-M-003 -020-MY3. We thank Richard Zeebe for a suggestion.

## REFERENCES

- Abbot, D. S., Webber, R. J., Hernandez, D. M., Hadden, S., & Weare, J. 2024, *ApJ*, 967, 121, doi: [10.3847/1538-4357/ad3e5f](https://doi.org/10.3847/1538-4357/ad3e5f)
- Baker, H. F. 1902, *Proc. London Math. Soc.*, s1-35, 333, doi: [10.1112/plms/s1-35.1.333](https://doi.org/10.1112/plms/s1-35.1.333)
- Baker, H. F. 1905, *Proc. London Math. Soc.*, s2-3, 24, doi: [10.1112/plms/s2-3.1.24](https://doi.org/10.1112/plms/s2-3.1.24)
- Blanes, S., & Casas, F. 2017, *A Concise Introduction to Geometric Numerical Integration*, Chapman & Hall/CRC Monographs and Research Notes in Mathematics (CRC Press)
- Campbell, J. 1896, *Proc. London Math. Soc.*, s1-28, 381, doi: [10.1112/plms/s1-28.1.381](https://doi.org/10.1112/plms/s1-28.1.381)
- Campbell, J. 1897, *Proc. London Math. Soc.*, s1-29, 14, doi: [10.1112/plms/s1-29.1.14](https://doi.org/10.1112/plms/s1-29.1.14)
- Chambers, J. E. 1999, *MNRAS*, 304, 793, doi: [10.1046/j.1365-8711.1999.02379.x](https://doi.org/10.1046/j.1365-8711.1999.02379.x)
- Channell, P. J., & Scovel, C. 1990, *Nonlinearity*, 3, 231
- Dehnen, W., & Hernandez, D. M. 2017, *MNRAS*, 465, 1201, doi: [10.1093/mnras/stw2758](https://doi.org/10.1093/mnras/stw2758)
- Duncan, M. J., Levison, H. F., & Lee, M. H. 1998, *AJ*, 116, 2067, doi: [10.1086/300541](https://doi.org/10.1086/300541)
- Dynkin, E. 1947 *Doklady Akademii Nauk SSSR*, 57, 323
- Fassò, F. 2005, *Acta Applicandae Mathematica*, 87, 101, doi: [10.1007/s10440-005-1139-8](https://doi.org/10.1007/s10440-005-1139-8)
- Gonçalves Ferrari, G., Boekholt, T., & Portegies Zwart, S. F. 2014, *MNRAS*, 440, 719, <https://arxiv.org/abs/1402.3325>
- Grimm, S. L., & Stadel, J. G. 2014, *ApJ*, 796, 23, doi: [10.1088/0004-637X/796/1/23](https://doi.org/10.1088/0004-637X/796/1/23)
- Hairer, E., Lubich, C., & Wanner, G. 2006, *Geometrical Numerical Integration*, 2nd edn. (Berlin: Springer Verlag)
- Hausdorff, F. 1906, *Ber. Verh. Sächs. Adak. Wiss.* 58, 19
- Hernandez, D. M., & Bertschinger, E. 2015, *MNRAS*, 452, 1934, doi: [10.1093/mnras/stv1439](https://doi.org/10.1093/mnras/stv1439)
- Hernandez, D. M., & Dehnen, W. 2017, *MNRAS*, 468, 2614, doi: [10.1093/mnras/stx547](https://doi.org/10.1093/mnras/stx547)
- Hernandez, D. M., & Dehnen, W. 2023, *MNRAS*, 522, 4639, doi: [10.1093/mnras/stad657](https://doi.org/10.1093/mnras/stad657)
- Hernandez, D. M., Zeebe, R. E., & Hadden, S. 2022, *MNRAS*, 510, 4302, doi: [10.1093/mnras/stab3664](https://doi.org/10.1093/mnras/stab3664)
- Javaheri, P., Rein, H., & Tamayo, D. 2023, *The Open Journal of Astrophysics*, 6, 29, doi: [10.21105/astro.2307.05683](https://doi.org/10.21105/astro.2307.05683)
- Kaib, N. A., & Raymond, S. N. 2025, *Icarus*, 439, 116632, doi: [10.1016/j.icarus.2025.116632](https://doi.org/10.1016/j.icarus.2025.116632)
- Kinoshita, H., Yoshida, H., & Nakai, H. 1991, *Celestial Mechanics and Dynamical Astronomy*, 50, 59
- Lee, M. H., Duncan, M. J., & Levison, H. F. 1997, in *Astronomical Society of the Pacific Conference Series*, Vol. 12, *Computational Astrophysics; 12th Kingston Meeting on Theoretical Astrophysics*, ed. D. A. Clarke & M. J. West, 32
- Leimkuhler, B., & Reich, S. 2004, *Simulating Hamiltonian Dynamics* (Cambridge University Press)
- Levison, H. F., & Duncan, M. J. 2000, *AJ*, 120, 2117, doi: [10.1086/301553](https://doi.org/10.1086/301553)
- Lu, T., Hernandez, D. M., & Rein, H. 2024, *MNRAS*, 533, 3708, doi: [10.1093/mnras/stae1982](https://doi.org/10.1093/mnras/stae1982)
- Nobili, A., & Roxburgh, I. W. 1986, in *Relativity in Celestial Mechanics and Astrometry. High Precision Dynamical Theories and Observational Verifications*, ed. J. Kovalevsky & V. A. Brumberg, Vol. 114, 105
- Rauch, K. P., & Hamilton, D. P. 2002, in *AAS/Division of Dynamical Astronomy Meeting*, Vol. 33, *AAS/Division of Dynamical Astronomy Meeting #33*, 08.02
- Rauch, K. P., & Holman, M. 1999, *AJ*, 117, 1087, doi: [10.1086/300720](https://doi.org/10.1086/300720)
- Rein, H., Brown, G., & Kanda, M. 2025, *The Open Journal of Astrophysics*, 8, 54745, doi: [10.33232/001c.154745](https://doi.org/10.33232/001c.154745)
- Rein, H., Dey, K., & Tamayo, D. 2026, *arXiv e-prints*, arXiv:2601.08019, doi: [10.48550/arXiv.2601.08019](https://doi.org/10.48550/arXiv.2601.08019)
- Rein, H., & Tamayo, D. 2019, *Research Notes of the AAS*, 3, 16, doi: [10.3847/2515-5172/aaff63](https://doi.org/10.3847/2515-5172/aaff63)
- Rein, H., Hernandez, D. M., Tamayo, D., et al. 2019, *MNRAS*, 485, 5490, doi: [10.1093/mnras/stz769](https://doi.org/10.1093/mnras/stz769)
- Saha, P., & Tremaine, S. 1992, *AJ*, 104, 1633, doi: [10.1086/116347](https://doi.org/10.1086/116347)
- Sanz-Serna, J., & Calvo, M. 1994, *Numerical Hamiltonian Problems*, 1st edn. (London: Chapman and Hall)
- Tamayo, D., Rein, H., Shi, P., & Hernandez, D. M. 2020, *MNRAS*, 491, 2885, doi: [10.1093/mnras/stz2870](https://doi.org/10.1093/mnras/stz2870)
- Tremaine, S. 2023, *Dynamics of Planetary Systems*
- Wisdom, J. 2015, *AJ*, 150, 127, doi: [10.1088/0004-6256/150/4/127](https://doi.org/10.1088/0004-6256/150/4/127)
- Wisdom, J., & Holman, M. 1991, *AJ*, 102, 1528, doi: [10.1086/115978](https://doi.org/10.1086/115978)
- Zeebe, R. E. 2015, *ApJ*, 798, 8, doi: [10.1088/0004-637X/798/1/8](https://doi.org/10.1088/0004-637X/798/1/8)